A Systematic Computational Study of the Reactions of HO_2 with RO_2: The $HO_2 + C_2H_5O_2$ Reaction

Hua Hou, Jicun Li, Xinli Song, and Baoshan Wang*

College of Chemistry and Molecular Sciences, Wuhan University, Wuhan, 430072, People's Republic of China

Received: September 5, 2005; In Final Form: October 17, 2005

The reaction of HO_2 with $C_2H_5O_2$ has been studied using the density functional theory (B3LYP) and the coupled-cluster theory [CCSD(T)]. The reaction proceeds on the triplet potential energy surface via hydrogen abstraction to form ethyl hydroperoxide and oxygen. On the singlet potential energy surface, the addition−elimination mechanism is revealed. Variational transition state theory is used to calculate the temperature-dependent rate constants in the range 200−1000 K. At low temperatures (e.g., below 300 K), the reaction takes place predominantly on the triplet surface. The calculated low-temperature rate constants are in good agreement with the experimental data. As the temperature increases, the singlet reaction mechanism plays more and more important role, with the formation of OH radical predominantly. The isotope effect of the reaction ($DO_2 + C_2D_5O_2$ vs $HO_2 + C_2H_5O_2$) is negligible. In addition, the triplet abstraction energetic routes for the reactions of HO_2 with 11 alkylperoxy radicals ($C_nH_mO_2$) are studied. It is shown that the room-temperature rate constants have good linear correlation with the activation energies for the hydrogen abstraction.

I. Introduction

Recently we have carried out a systematic theoretical study of the reactions of HO_2 with the alkylperoxy radicals (RO_2).[1,2] The $HO_2 + RO_2$ reaction is important in the global atmospheric chemistry. Both the reaction mechanisms and kinetic data need to be known for the $HO_2 + RO_2$ reactions in the atmospheric models and in the development of structure−activity relationships (SAR). In this paper, the $HO_2 + C_2H_5O_2$ reaction is investigated by various ab initio theories. In addition, an SAR analysis is presented for 11 analogous alkylperoxy ($C_nH_mO_2$) reactions.

There are numerous experimental studies on the $HO_2 + C_2H_5O_2$ reaction. Mechanistically, it has been shown that the $HO_2 + C_2H_5O_2$ reaction involves a single pathway giving exclusively ethyl hydroperoxide (C_2H_5OOH) at room temperature.[3−5] No evidence was found for acetaldehyde (CH_3CHO). The kinetics of the $HO_2 + C_2H_5O_2$ reaction have been measured a few times covering the temperature range from 210 to 480 K.[6−10] The overall rate constants show negative temperature dependence with reported apparent activation energy (E_a) values between −5.4 and −10.5 kJ/mol. The room-temperature rate constant is approximately 8×10^{-12} cm^3 molecule^{-1} s^{-1}. For the reactions of the larger alkylperoxy radicals, it was found that the rate constants increase with the size of the RO_2 radicals, from nearly 5×10^{-12} cm^3 molecule^{-1} s^{-1} for CH_3O_2, up to a limit of about 22×10^{-12} cm^{3}molecule^{-1} s^{-1} for the straight-chain C_{14} alkylperoxy radicals.[10]

To our knowledge there is no theoretical study of the title reaction. In the present paper, using high-level ab initio calculations, we first answer the question why the production of ethyl hydroperoxide is the only channel observed experimentally. Second, we investigate how the rate constant changes with the temperature. The high-temperature kinetics will be predicted together with reasonable explanations of the experimental low-temperature rate constant data. The isotope effect ($DO_2 + C_2D_5O_2$ vs $HO_2 + C_2H_5O_2$) will be addressed as well. Third, an SAR model will be developed to gain some insight into the room-temperature kinetics for the reactions of HO_2 with the unsubstituted alkylperoxy radicals.

II. Computational Methods

The $HO_2 + C_2H_5O_2$ reaction occurs on both triplet and singlet potential energy surfaces. The geometries of reactants, intermediates (IM), transition states (TS), and products were fully optimized using the B3LYP density functional theory[11] with the standard triple-ζ 6-311G(d,p) basis set. Harmonic vibrational frequencies were calculated at the same level of theory for the characterization of stationary points (minimum or transition state) and for the zero-point energy (ZPE) corrections. The intrinsic reaction coordinates were routinely calculated for the predicted transition states.

On the basis of the B3LYP/6-311G(d,p) optimized geometries, two higher-level ab initio methods were used to calculate the single-point energies. The first method is the unrestricted coupled-cluster theory with single, double, and noniterative triple excitations [UCCSD(T)][12] with Dunning's correlation-consistent double-ζ basis set (cc-pVDZ).[13] The second method is the restricted CCSD(T) theory[14] with the complete basis set (CBS) extrapolation using the expressions:[15,16]

$$E_{HF}^{X} = E_{HF}^{\infty} + ae^{-bX}, \Delta E_{corr}^{X} = \Delta E_{corr}^{\infty} + \frac{c}{X^3}$$

where $X = 2, 3, 4$ are for the Dunning's cc-pVDZ, cc-pVTZ, cc-pVQZ basis sets, and a, b, c are extrapolation parameters. Gaussian03 and Molpro programs[17,18] were employed to carry out all ab initio calculations in this work.

The kinetic parameters were calculated using the statistical transition state theory. The barrierless reaction paths are treated using the variational method. The details and references are given in Section III.4.

* Corresponding author. Email: wangb@chem.whu.edu.cn. Fax: 86-27-6875-4067.

10.1021/jp0550098 CCC: $30.25
Published on Web 11/17/2005

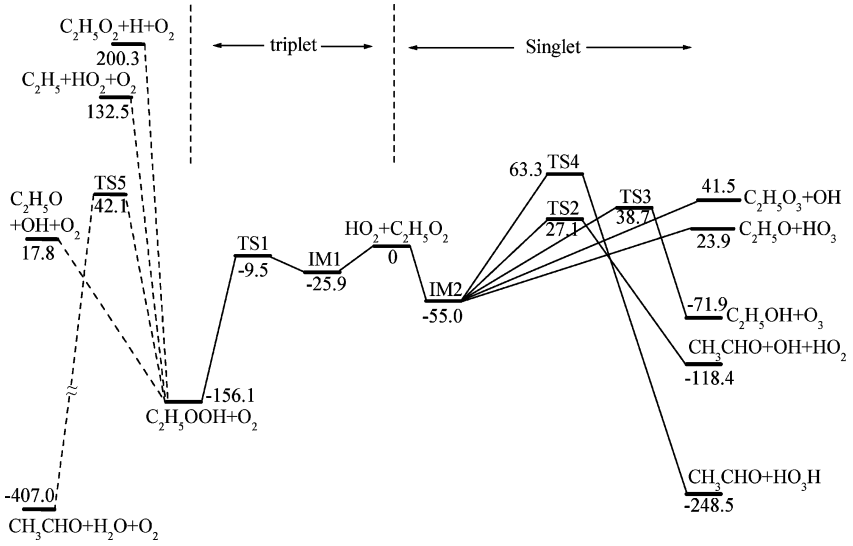

Figure 1. The energetic routes for the $HO_2 + C_2H_5O_2$ reaction at the RCCSD(T)/CBS level of theory using the B3LYP/6-311G(d,p) optimized geometries. The unimolecular decomposition of C_2H_5OOH is shown by the dashed lines. Energies are in the unit of kJ/mol.

TABLE 1: Zero-Point Energy Corrected Relative Energies for the $HO_2 + C_2H_5O_2$ Reaction (ΔE, in kJ/mol)[a]

species	ΔE B3LYP/6-311G(d,p)	ΔE CCSD(T)/cc-pVDZ	ΔE RCCSD(T)/CBS	ΔH^{298} RCCSD(T)/CBS	ΔH^{298} (exptl) [b]
IM1	−33.7 (−29.7)	−34.1 (−31.9)	−25.9 (−24.5) [−27.0]	−26.4 (−24.9)	
TS1	−33.6 (−2.8)	−17.7 (−2.4)	−9.5 (7.2) [−8.7]	−12.2 (3.1)	
$C_2H_5OOH + O_2$	−135.2 (−216.7)	−157.6 (−164.3)	−156.1 (−159.7) [−156.6]	−156.1 (−159.5)	−161.5 ± 26.4
IM2	−23.1	−37.2	−55.0 [−55.9]	−58.8	
TS2	53.4	38.2	27.1 [30.9]	23.4	
$CH_3CHO + OH + HO_2$	−96.4	−116.5	−118.4 [−114.1]	−112.8	−101.3 ± 17.6
TS3	73.1	45.9	38.7 [41.3]	33.2	
$C_2H_5OH + O_3$	−12.0	−53.1	−71.9 [−72.3]	−73.6	−79.1 ± 15.5
TS4	93.9	72.5	63.3 [66.4]	60.0	
$CH_3CHO + HO_3H$	−212.5	−224.9	−248.5 [−247.7]	−249.2	−241.4 ± 13.8
$C_2H_5O + HO_3$	20.0	23.4	23.9 [25.7]	24.8	22.2 ± 17.6
$C_2H_5O_3 + OH$	53.9	43.1	41.5 [43.8]	43.6	56.5 ± 22.2
$C_2H_5O + OH + O_2$	18.7	−5.1	17.8 [22.0]	23.8	33.9 ± 18.0
TS5	60.7	32.2	42.1 [46.6]	41.7	
$CH_3CHO + H_2O + O_2$	−371.6	−396.3	−407.0 [−403.8]	−401.4	−394.1 ± 13.8
$C_2H_5 + HO_2 + O_2$	119.0	108.2	132.5 [136.4]	138.4	148.5 ± 11.7
$C_2H_5O_2 + H + O_2$	191.8	165.9	200.3 [208.4]	199.0	204.2 ± 3.3

[a] The data in parentheses are calculated on the basis of the MP2(full)/6-311G(d,p) optimized geometries. The data in brackets correspond to the $DO_2 + C_2D_5O_2$ reaction. [b] Obtained using the enthalpies of formation taken from ref 19.

III. Results and Discussion

The energetics for the mechanistic pathways for the $HO_2 + C_2H_5O_2$ reaction are shown in Figure 1. These pathways consist of the single hydroperoxide product channel on the triplet surface and the multiple radical channels on the singlet surface. For completeness, the secondary reaction of the ethyl hydroperoxide product is included as well. As Figure 1 shows, the triplet reaction path, $HO_2 + C_2H_5O_2 \rightarrow$ IM1 $\rightarrow$ TS1 $\rightarrow C_2H_5OOH + O_2$, involves the lowest barrier and is exothermic significantly. It is conceivable that the C_2H_5OOH is the major product at low temperatures, in accordance with the experimental observation.[3−5] The relative energies with respect to the $HO_2 + C_2H_5O_2$ reactants at various levels of theory are summarized in Table 1.

In the following sections, the overall reaction mechanism will be discussed briefly using the RCCSD(T)/CBS//B3LYP/6-311G(d,p) data in Section III.1. Then the influence of the levels of theory on the geometries and energetic routes is discussed in Section III.2. The kinetic calculations are presented in Section III.3. Finally, some concluding remarks are given in Section IV.

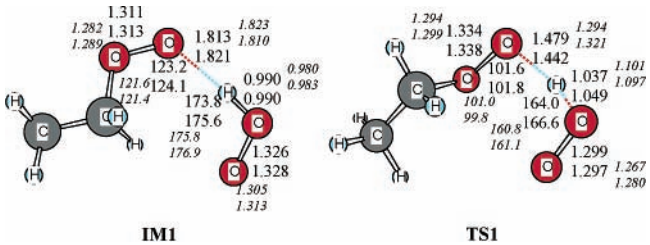

Figure 2. The optimized geometries for IM1 and TS1 (triplet) at the B3LYP/6-311G(d,p) level of theory (upper cases) and at the B3LYP/6-311++G(2d,2p) level of theory (lower cases). The MP2/6-311G(d,p) and MP2/6-311++G(2d,2p) optimized parameters are shown in Italics. Bond distances are in Å and bond angles are in degrees.

1. Reaction Mechanism. *1.1. Triplet Abstraction.* A hydrogen abstraction reaction takes place on the triplet surface via a precursor (intermediate, IM1) and a transition state (TS1). The geometries of IM1 and TS1 are shown in Figure 2.

IM1 is a hydrogen bond complex. The hydrogen bonding occurs between the hydrogen atom of HO_2 and the terminal oxygen atom of $C_2H_5O_2$, with a distance of about 1.8 Å. The hydrogen-bond angle OHO is almost linear. The binding energy

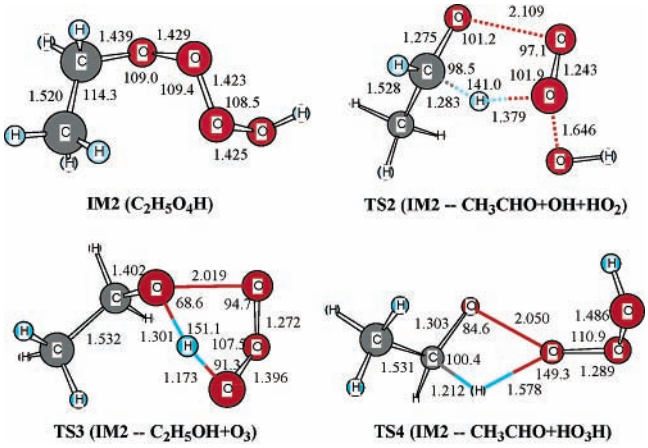

Figure 3. The optimized geometries for IM2 ($C_2H_5O_4H$) and TS2−TS4 (singlet) at the B3LYP/6-311G(d,p) level of theory. Bond distances are in Å and bond angles are in degrees.

is about 25.9 kJ/mol. TS1 is an early barrier. The breaking HO bond is slightly stretched by less than 0.1 Å, and the forming OH bond is 1.5 times longer than the equilibrium distance. Although TS1 lies above IM1 by about 16.4 kJ/mol, the energy of TS1 is still about 9.5 kJ/mol lower than the total energy of the $HO_2 + C_2H_5O_2$ reactants.

1.2. Addition-Elimination Mechanism. The addition−elimination mechanism is revealed for the singlet potential energy surface. The association of HO_2 with $C_2H_5O_2$ produces a tetroxide intermediate, $C_2H_5O_4H$. The most stable conformation of $C_2H_5O_4H$ (denoted as IM2) is shown in Figure 3. Three OO bonds of $C_2H_5O_4H$ have the similar distances around 1.4 Å with the OOOO dihedral angle of about 81°. IM2 is about 55 kJ/mol more stable with respect to the initial $HO_2 + C_2H_5O_2$ reactants.

Analogous to the tetroxide intermediates in the other $HO_2 + RO_2$ reactions,[1,2] IM2 can decompose to form various products via a few ring-like transition states. TS2 is a five-membered-ring structure. The breaking of the two OO bonds is accompanied by the hydrogen atom migration from the CH_2 group to the O atom, forming CH_3CHO, OH, and HO_2. In fact, TS2 represents a HO_2-mediated decomposition mechanism for $C_2H_5O_2$ because the HO_2 radical is recovered from the final products. The barrier for TS2 is about 82.1 kJ/mol with respect to IM2. TS3 is the other five-member-ring structure, leading to ethanol and ozone. The barrier for TS3 is higher than that for TS2 by about 11.6 kJ/mol. Because of the small strain in the five-member-ring, the barriers for TS2 and TS3 are relatively low, in comparison with the four-membered-ring transition state TS4. However, the formation of CH_3CHO and HO_3H via TS4 is the most exothermic channel on the singlet surface.

There are two simple OO bond fission channels starting from IM2, forming $C_2H_5O + HO_2$ and $C_2H_5O_3 + OH$, respectively. Both channels are endothermic. No transition state is expected for either radical product channel. Interestingly, the scan of the OO bond-breaking potential curve using the partial optimization technique [e.g., the breaking OO bond distances are fixed and the other geometrical parameters are optimized at the B3LYP/6-311G(d,p) level of theory] always leads to the decomposition into $CH_3CHO + OH + HO_2$, rather than the $C_2H_5O + HO_3$ asymptote or the $C_2H_5O_3 + OH$ asymptote. The reason is the flexible R−O−O−O−O−H skeleton of IM2 in which three OO bonds rotate during the optimization.

As shown in Figure 1, all the barriers on the singlet surface are well-above the $HO_2 + C_2H_5O_2$ reactants. It is foreseeable

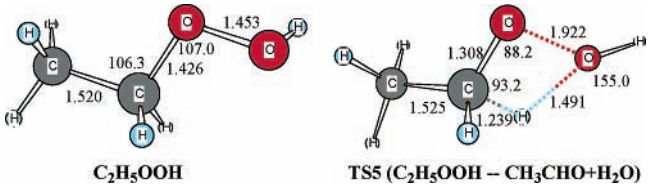

Figure 4. The optimized geometries for C_2H_5OOH and TS5 (leading to CH_3CHO and H_2O) at the B3LYP/6-311G(d,p) level of theory. Bond distances are in Å and bond angles are in degrees.

that these mechanisms only play an observable role at elevated temperatures.

1.3. Unimolecular Decomposition of C_2H_5OOH. On the triplet potential energy surface, the formation of C_2H_5OOH and O_2 is highly exothermic. Presumably, a fraction of exothermicity might be deposited into the polyatomic hydroperoxide molecule and make it internally excited. Therefore, the unimolecular reaction of C_2H_5OOH (see Figure 4 for its geometry, and the reaction routes are indicated by the dashed lines in Figure 1) has been studied in order to estimate the lifetime of the C_2H_5OOH product molecule.

The most favorable reaction mechanism is the simple OO bond cleavage channel, forming C_2H_5O and OH with an endothermicity of about 174 kJ/mol without additional barrier. As shown in Figure 1, the total energy of $C_2H_5O + OH(+O_2)$ is still 17.8 kJ/mol higher than that of the $HO_2 + C_2H_5O_2$ reactants. It appears that there is not enough available energy to make the C_2H_5OOH molecule decompose. Therefore, C_2H_5OOH should be a stable final product in the $C_2H_5O_2 + HO_2$ reaction as observed in the experiments.[3−5]

The decomposition of C_2H_5OOH into CH_3CHO and H_2O is highly exothermic by about 250 kJ/mol. However, this channel undergoes via a four-center transition state TS5 (see Figure 4). The barrier is as high as 198 kJ/mol. The other two simple CO and OH bond fission channels, forming $C_2H_5 + HO_2$ and $C_2H_5O_2 + H$, respectively, are highly endothermic and thus of no importance.

In summary, all the low-lying reaction routes for the $HO_2 + C_2H_5O_2$ reaction are reported in Figure 1. For completeness, a few high-barrier reaction routes are provided as the Supporting Information (see Figure S1). At normal atmospheric temperatures (e.g., below 300 K), evidently the dominant mechanism is the abstraction on a triplet surface, producing C_2H_5OOH and O_2 molecules without a *net* barrier. This qualitative result is in good agreement with the experimental measurements in the range $T = 282-314$ K. The yield of C_2H_5OOH was measured to be $(93 \pm 10)\% - (104 \pm 5)\%$ using FTIR spectroscopy.[3−5] The quantitative kinetic data will be presented in Section III.3.

In addition, the isotope effect was studied for the $DO_2 + C_2D_5O_2$ reaction. The relative energies are listed in Table 1 (see the data in brackets). Apparently, the isotope substitution increases the barrier heights slightly for all product channels. The relative orders of the energetic routes for the $DO_2 + C_2D_5O_2$ reaction remain unchanged. Therefore, the isotope effect is nearly negligible.

2. Assessment of the ab Initio Energies and Geometries. Table 1 lists the energies calculated at various levels of theory. The good quality of the RCCSD(T)/CBS energies is evident. The calculated heats of reaction at 298.15 K for 10 product channels are in good agreement with the experimental data.[19] In our previous study, the UCCSD(T)/cc-pVDZ level of theory was suggested to be the most appropriate method to study the $HO_2 + RO_2$ reaction in the consideration of the balance between computational efficiency and cost.[1,2] For the $HO_2 + C_2H_5O_2$

reaction, the UCCSD(T)/cc-pVDZ level of theory still shows good performance in comparison with the RCCSD(T)/CBS data. Although the depth of the well IM2 is too shallow at the UCCSD(T)/cc-pVDZ level of theory, the relative orders of the stationary points are the same with the two levels of theory. However, the UCCSD(T)/cc-pVDZ level of theory performs worse for the unimolecular decomposition reaction of C_2H_5OOH. For example, the $C_2H_5O + OH(+O_2)$ channel was calculated to be slightly exothermic (−5.1 kJ/mol), in contrast to the RCCSD(T)/CBS value (17.8 kJ/mol) and the experimental endothermicity (33.9 ± 18.0 kJ/mol).[19] Moreover, the calculated endothermicities for the $C_2H_5 + HO_2(+O_2)$ and $C_2H_5O_2 + H(+O_2)$ channels are significantly smaller than the experimental data. Fortunately, the main conclusions on the reaction mechanism are not affected by these deficiencies. It is worth noting that the experimental heats of reaction themselves involve significant uncertainties. In many cases, the experimental uncertainties are so large that they can cover much of the difference between the RCCSD(T)/CBS and UCCSD(T)/cc-pVDZ calculations. As a result, it becomes difficult to assess the accuracy of the theoretical energies. By experience, the RCCSD(T)/CBS data are supposed to be more reliable than the UCCSD(T)/cc-pVDZ results.

The influence of the geometry change with the levels of theory and the basis sets has been checked for the abstraction reaction on a triplet surface. The geometries of IM1 and TS1 were optimized using the all-electron second-order Möller−Plesset perturbation theory (MP2)[20] with the basis sets of 6-311G(d,p). Furthermore, a larger basis set, namely, 6-311++G(2d,2p), was used for both B3LYP and MP2 optimizations. The geometrical data are shown in Figure 2 for comparison. Two conclusions can be drawn. First, the geometries are nearly identical for the basis sets with either B3LYP or MP2 theory. Changes in the geometry from B3LYP/6-311G(d,p) [or MP2/6-311G(d,p)] to B3LYP/6-311++G(2d,2p) [or MP2/6-311++G(2d,2p)] are only minimal for both IM1 and TS1. Second, the geometry of TS1 changes dramatically from B3LYP to MP2 levels of theory while that of IM1 is nearly unchanged. At the MP2/6-311G(d,p) level of theory, TS1 becomes a much later barrier because the forming O···H bond is shortened significantly from 1.48 to 1.29 Å. As a result, at the RCCSD(T)/CBS//MP2/6-311G(d,p) level of theory, the barrier height for TS1 is 7.2 kJ/mol *above* the $HO_2 + C_2H_5O_2$ reactants, in contrary to the RCCSD(T)/CBS//B3LYP/6-311G(d,p) result (e.g., 9.5 kJ/mol *below* the reactants). Another apparent difference is the imaginary frequency of TS1 obtained at the B3LYP/6-311G(d,p) and MP2/6-311G(d,p) levels of theory, that is, 231 cm^{-1} versus 1925 cm^{-1}. The former is nearly nine times smaller than the latter. In short, TS1 appears to be sensitive to the level of theory used in the calculation.

Ideally, the higher level of theory such as CCSD(T) should be used to check the geometry change. However, such a calculation is beyond our computation capability. The experimental studies on the rate constants of the $HO_2 + C_2H_5O_2$ reaction found a negative temperature dependence with the apparent activation energy between −5.4 and −10.5 kJ/mol.[6−10] Usually this implies that the $HO_2 + C_2H_5O_2$ reaction should have at least one channel involving an energy barrier below the energy of the reactants. The calculated barrier for TS1 (−9.5 kJ/mol) at the RCCSD(T)/CBS//B3LYP/6-311G(d,p) level of theory happens to be in the experimental range whereas that at the RCCSD(T)/CBS//MP2/6-311G(d,p) level of theory is obviously overestimated. Therefore, it appears that the B3LYP optimized geometries might be more reliable than the MP2 ones.

TABLE 2: Morse Potential Parameters Used in the Kinetic Calculation for the $HO_2 + C_2H_5O_2$ Reaction

bonds	ν (cm^{-1})[a]	D_e (kJ/mol)[b]	R_e (Å)[a]	β ($Å^{-1}$)
$C_2H_5OO-OOH$	595.5	71.5	1.423	3.509
$C_2H_5O-OOOH$	621.6	100.0	1.429	2.629
$C_2H_5OOO-OH$	921.2	115.9	1.425	3.324

[a] At the B3LYP/6-311G(d,p) level of theory. [b] At the RCCSD(T)/CBS//B3LYP/6-311G(d,p) level of theory.

Of course, the larger imaginary frequency of TS1 at the MP2/6-311G(d,p) level of theory implies that the rate may be increased through tunneling, but the following kinetic calculations indicate that such a compensation is insignificant.

3. Kinetic Simulation. The rate constants for the $HO_2 + C_2H_5O_2$ reaction have been calculated using transition state theory as a function of temperatures (200−1000 K) at 760 Torr of air (e.g., the pressure used in the experiments). The deactivation rates of the intermediates (IM1 and IM2) were estimated using the exponential-down energy transfer mode.[21] The empirical energy transfer parameters, $\langle \Delta E \rangle_{down} = -100$ cm^{-1}, and the Lennard−Jones (LJ) collisional efficiency parameters, $\epsilon = 100$ K, $\sigma = 5.0$ Å, were employed in the calculation. Note that the rate constant is insensitive to the above parameters at the pressure of our interest. The contribution from the stabilization of IM1 or IM2 to the overall reaction rate is of significance only at very low temperatures and high pressures.

For the tight transition states (e.g., TS1−TS4), the rigid rotor harmonic oscillator approximation was used to evaluate sum and densities of states at the energy and angular momentum resolved level. Quantum tunneling was included using the Eckart formula,[22] which is determined by three parameters: the imaginary frequency, the barrier height, and the reaction exothermicity.

The hydrogen bond interaction (IM1) at the entrance channel of the triplet surface was described by a Lennard−Jones (12−10) potential with the well-depth of 33.1 kJ/mol and the equilibrium distance of 1.813 Å. For the singlet reaction mechanism, there are three barrierless channels, namely, the association of HO_2 with $C_2H_5O_2$, the decomposition of IM2 to produce $C_2H_5O + HO_3$ and $C_2H_5O_3 + OH$. The interaction potential between the two fragments was described by summing the bonding potential for the reacting OO bonds and the pairwise LJ(12−6) nonbonding potentials for the rest of interfragment atoms. In principle, the bonding potential should be calculated using ab initio methods, however, such a calculation cannot be afforded at present. Moreover, the calculations of the potential curves for the OO bond-breaking paths of $C_2H_5O-O_3H$ and $C_2H_5O_3-OH$ are unsuccessful because the partial optimization cannot lead to the desired products. Therefore, the OO bonding interaction was estimated using the Morse potential, i.e., $V_M = D_e[1 - e^{-\beta}(R - R_e)]^2 - D_e$. The binding energy ($D_e$, excluding ZPE) and equilibrium bond distance (R_e) are taken directly from the ab initio calculations. The range parameter, β, was calculated using the formula, $\beta = 2\pi c\tilde{\nu}\sqrt{\mu/2D_e}$, where the vibrational frequency $\tilde{\nu}$ and the reduced mass μ were obtained from the vibrational analysis at the B3LYP/6-311G(d,p) level of theory. The empirical LJ(12−6) potential parameters for H, C, and O atoms were taken directly from the literature.[23] The Morse parameters are summarized in Table 2. The evaluation of the number and density of states of the above barrierless paths were carried out variationally using the flexible transition state theory[24] as implemented in the Variflex program.[25]

As expected, the rate constants obtained from the parametrized kinetic simulation might have large uncertainties.

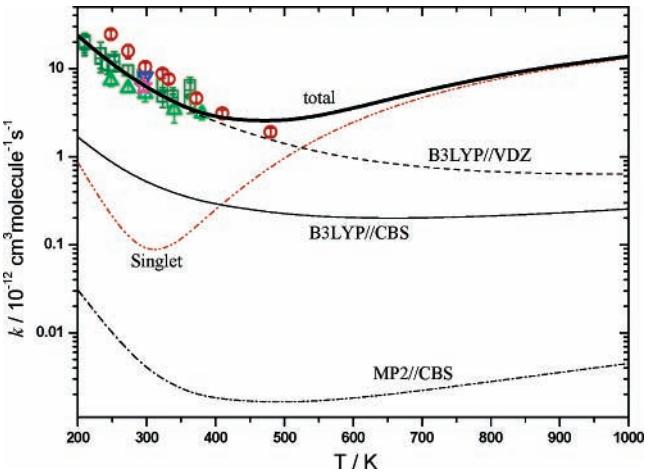

Figure 5. The theoretical rate constants for the $HO_2 + C_2H_5O_2$ reaction. The experimental data: ☆ ref 6. △ ref 7. ○ ref 8. □ ref 9. ▽ ref 10. Dash−dot-dotted line (Singlet): the rate constants for the addition−elimination reaction on the singlet surface using the B3LYP/6-311G(d,p) optimized geometries and vibrational frequencies and the RCCSD(T)/CBS energies. Dash−dotted line (MP2//CBS): the rate constants for the triplet abstraction path using the MP2/6-311G(d,p) optimized geometries and vibrational frequencies and the RCCSD(T)/CBS energies. Thin solid line (B3LYP//CBS): the rate constants for the triplet abstraction path using the B3LYP/6-311G(d,p) optimized geometries and vibrational frequencies and the RCCSD(T)/CBS energies. Dashed line (B3LYP//VDZ): the rate constants for the triplet abstraction path using the B3LYP/6-311G(d,p) optimized geometries and vibrational frequencies and the UCCSD(T)/cc-pVDZ energies. Solid line (total): the total rate constants summing "singlet" with "B3LYP//VDZ".

However, our calculations on the barrier heights and heats of reaction, which are the most critical parameters for the evaluation of the rate constants, should be sound. Therefore, the semiempirical kinetic simulation is meaningful to investigate the temperature dependence of the overall and individual rate constants. More interestingly, it is useful to assess the relative importance of the singlet and triplet reaction mechanisms and the relative importance of each with the temperature.

The calculated rate constants and the experimental data are shown in Figure 5 for comparison. It is found that the rate constants for both triplet and singlet reaction mechanisms decrease first at lower temperatures and then increase with the elevated temperatures. Three calculations have been performed for the triplet reaction path using three types of ab initio data, namely, the RCCSD(T)/CBS energetics based on the MP2/6-311G(d,p) optimized geometrical parameters and frequencies (denoted as MP2//CBS as shown by the dash−dotted line in Figure 5), the RCCSD(T)/CBS energetics based on the B3LYP/6-311G(d,p) optimized geometrical parameters and frequencies (denoted as B3LYP//CBS as shown by the thin solid line in Figure 5), and the B3LYP/6-311G(d,p) optimized geometrical parameters and frequencies with the UCCSD(T)/cc-pVDZ energetics (denoted as B3LYP//VDZ as shown by the dashed line in Figure 5). As for the singlet reaction pathways, the rate constants were calculated at the B3LYP//CBS level. It is worth noting that the temperature trends in the B3LYP//VDZ, B3LYP//CBS, and MP2//CBS triplet calculations are similar. Evidently, the B3LYP//VDZ calculation gives the largest rate constants, which are in good agreement with the experimental data. Both B3LYP//CBS and MP2//CBS rate constants are much smaller than the experimental data.[6−10] This result is understandable because the B3LYP//VDZ calculation gives the lowest barrier for TS1 (−17.7 kJ/mol), while the B3LYP//CBS barrier for TS1 is about 8 kJ/mol higher. The MP2//CBS barrier is even as high as +7.2 kJ/mol with respect to the $HO_2 + C_2H_5O_2$ reactants. Certainly, the better performance of B3LYP//VDZ than B3LYP//CBS may be just a coincidence or due to the cancellation of errors because the latter is thought to be more reliable. It is notable that the activation energy of TS1 with respect to IM1 is the same between the B3LYP//VDZ and the B3LYP//CBS levels of theory, namely, 16.4 kJ/mol as shown in Table 1.

The sum of B3LYP//VDZ rate constants for the triplet reaction mechanism with the singlet contribution gives the total rate constants for the $HO_2 + C_2H_5O_2$ reaction (see the thick solid line in Figure 5). The theoretical data are in reasonable agreement with the experimental data in the temperature range from 200 to 400 K.[6−10] Evidently, the reaction on the triplet surface to form $C_2H_5OOH + O_2$ via hydrogen abstraction dominates the overall reaction below 400 K. The contribution of the singlet mechanism is negligible at these temperatures (Note that only the collisional formation of the tetroxide molecule is significant. See Figure S2 in the Supporting Information). At temperatures above 400 K, the contribution from the singlet mechanism increases rapidly, while the triplet reaction pathway becomes relatively less important (Note that the formation of $C_2H_5O + HO_3$ dominates the reaction). As a result, the total rate constants increase with the temperatures $T > 400$ K. Since there is no high-temperature experimental data with which to compare, the present theoretical prediction on the change of mechanism with the temperature needs to be validated by new experiments. It is worth noting that the high-temperature reaction on the singlet surface produces $C_2H_5O + HO_3$ predominantly. The other two minor channels are the formation of $C_2H_5O_3 + OH$ and $CH_3CHO + OH + HO_2$. Since neither HO_3 nor $C_2H_5O_3$ is stable energetically, they might decompose quickly to form the final products $HO + O_2$ or $C_2H_5O + O_2$. It is notable that all these channels produce OH radicals. Therefore, it may be concluded that OH is the principal product of the $HO_2 + C_2H_5O_2$ reaction at high temperatures (e.g., above 500 K). Although there is no direct experimental observation on the product distribution of the $HO_2 + C_2H_5O_2$ reaction at high temperatures, it is worth noting that Kaiser suggested that the $HO_2 + C_2H_5O_2$ reaction might proceed directly to $C_2H_5O + OH + O_2$ in order to explain the yields of H_2O and H_2O_2 in his study of the oxidation of propionaldehyde.[26] More interestingly, the same trend and magnitude as the present results (e.g., Figure 5 and also Figure S2) has been observed by Kaiser for the rate constants of the $C_2H_5O + OH + O_2$ product channel at $T = 400-700$ K.[27]

4. Structure−Activity Relationships Study. The reactions of HO_2 with a series of alkylperoxy radicals have been studied in order to develop structure−activity relationships and thus to understand the characteristics of the unsubstituted alkylperoxy radicals. Since we are particularly interested in the atmospheric importance of the $HO_2 + RO_2$ reactions, only the reaction route on the triplet potential energy surface was considered because it is the most important mechanism at normal atmospheric temperatures (e.g., below 300 K). C_1-C_{10} alkylperoxy radicals including neo-$C_5H_{11}O_2$ and cyc-$C_6H_{11}O_2$ have been studied using the B3LYP/6-311G(d,p) optimized geometries and the RCCSD(T)/cc-pVDZ single-point energies. The distance of the hydrogen bond of the weakly bonded complex (IM1), the distances of the forming ROO···H bond and the breaking H···O_2 bond of the transition state (TS1), together with the binding energy of IM1, the barrier height, and the exothermicity are listed in Table 3. Two conclusions could be drawn from these ab initio data.

First, the geometrical data show convergence as the size of the RO_2 increases. For example, the distance of the hydrogen

TABLE 3: Summary of the ab Initio Results for the $HO_2 + C_nH_mO_2$ Reactions[a]

$C_nH_mO_2$	R_{HB} (Å)	R_{HO} (Å)	R_{OH} (Å)	ΔE_{IM1} (B3LYP)	$\Delta E'_{IM1}$ (RCC)	ΔE_{TS1} (B3LYP)	$\Delta E'_{TS1}$ (RCC)	E_a (RCC)	ΔH_r (B3LYP)	$\Delta H_r'$ (RCC)
CH_3O_2	1.824	1.509	1.030	−32.1	−31.5	−31.0	−13.0	18.5	−136.5	−160.0
$C_2H_5O_2$	1.813	1.479	1.037	−33.7	−33.6	−33.6	−14.5	19.0	−135.2	−159.4
$C_3H_7O_2$	1.811	1.476	1.038	−34.1	−34.0	−33.9	−14.6	19.3	−135.1	−159.5
$C_4H_9O_2$	1.810	1.475	1.038	−34.2	−34.2	−33.9	−14.8	19.4	−135.1	−159.4
$C_5H_{11}O_2$	1.809	1.474	1.038	−34.5	−34.6	−34.5	−15.4	19.1	−135.0	−159.4
$C_6H_{13}O_2$	1.808	1.472	1.039	−34.4	−34.5	−34.6	−15.4	19.1	−135.0	−159.4
$C_7H_{15}O_2$	1.809	1.472	1.038	−34.5	-	−34.7	-	-	−134.9	-
$C_8H_{17}O_2$	1.809	1.472	1.038	−34.7	-	−35.0	-	-	−134.9	-
$C_{10}H_{21}O_2$	1.809	1.471	1.039	−35.0	-	−35.3	-	-	−134.9	-
neo-$C_5H_{11}O_2$	1.809	1.455	1.043	−34.1	−34.2	−34.3	−13.8	20.4	−134.6	−159.5
cyc-$C_6H_{11}O_2$	1.793	1.451	1.045	−36.9	−38.7	−35.4	−15.3	23.4	−132.9	−157.9

[a] R_{HB}: the hydrogen bond distance in the intermediate IM1; R_{HO}: the distance of the forming H···O bond in the abstraction transition state TS1; R_{OH}: the distance of the breaking O···H bond in TS1. ΔE_{IM1}: the B3LYP/6-311G(d,p) calculated binding energy (in kJ/mol) of IM1 with respect to the $HO_2 + RO_2$ reactants; $\Delta E'_{IM1}$: the RCCSD(T)/cc-pVDZ calculated binding energy (in kJ/mol) of IM1; ΔE_{TS1}: the B3LYP/6-311G(d,p) calculated barrier height (in kJ/mol) of TS1 with respect to the $HO_2 + RO_2$ reactants; $\Delta E'_{TS1}$: the RCCSD(T)/cc-pVDZ calculated barrier height (in kJ/mol) of TS1; E_a: the activation barrier (in kJ/mol) of TS1 with respect to IM1; ΔH_r: the B3LYP/6-311G(d,p) calculated heat of reaction; $\Delta H_r'$: the RCCSD(T)/cc-pVDZ calculated heat of reaction.

bond of IM1 is converged to 1.809 Å for the straight-chain C_1 to C_{10} peroxy radicals. The two reacting HO bonds are converged to 1.472 and 1.038 Å. The heat of reaction is converged to −159 kJ/mol. Note that the neo-C_5 and cyc-C_6 peroxy radicals are apparently different from the straight-chain peroxy radicals in view of geometries and energetics.

Second, the RCCSD(T)/cc-pVDZ and B3LYP/6-311G(d,p) levels of theory give similar binding energies for IM1. The binding energy of IM1 (D_0) has a good linear relationship with the distance of the hydrogen bond (R_{HB}), e.g., D_0 (kJ/mol) = 314.1−154.6 × R_{HB} (Å). However, the calculated barrier heights are apparently different between the two levels of theory. As mentioned above, the transition state is very sensitive to the ab initio level of theory used in the calculation. Moreover, the correlation between the barrier heights and the geometrical parameters of the transition state is not good.

It was found that the RCCSD(T)/cc-pVDZ calculated activation energies (E_a) have a good linear relationship with the room-temperature rate constants. As far as we know, the rate constants have been well established experimentally for only six reactions, i.e., the reactions of CH_3O_2,[10,28−36] $C_2H_5O_2$,[6−10] neo-$C_5H_{11}O_2$, cyc-$C_6H_{11}O_2$, $C_{10}H_{21}O_2$, and $C_{14}H_{29}O_2$ peroxy radicals with the HO_2 radicals.[10] Unfortunately, we cannot treat the peroxy radicals with sizes beyond C_6 using the RCCSD(T)/cc-pVDZ level of theory. Therefore, only four rate constants were used in the correlation. The results are shown in Figure 6. The least-squares linear relationship is as follows:

$$k\,(10^{-12}\ \mathrm{cm^3\,molecule^{-1}\,s^{-1}}) = 4.06 \times E_a\,(\mathrm{kJ/mol}) - 69.36$$

The correlation coefficient is 0.99. Based on this linear relationship, the rate constants for C_3, C_4, C_5, C_6 peroxy radical reactions are estimated to be 9.12, 9.46, 8.27, and 8.27 ($\times 10^{-12}$ cm^3 $molecule^{-1}$ s^{-1}), respectively. On the other hand, the activation barriers are estimated to be 21.8 and 22.3 kJ/mol for the C_{10} and C_{14} peroxy radical reactions.

It should be noted that the difference of the activation energies between the peroxy radicals reactions is relatively small, e.g., only a few kJ/mol, which is comparable with (or even smaller than) the uncertainty of the theoretical activation energy. Therefore, it might be too dangerous to use the activation energy as a correlation variable. For the same reason, we cannot give the uncertainty for either predicted rate constant or activation energy. The smaller rate constants for the C_5, C_6 peroxy radical reactions than the C_3 and C_4 reactions might be an artifact. Of course, the theoretical data from the SAR study are waiting for the validation by new experiments and more advanced computations.

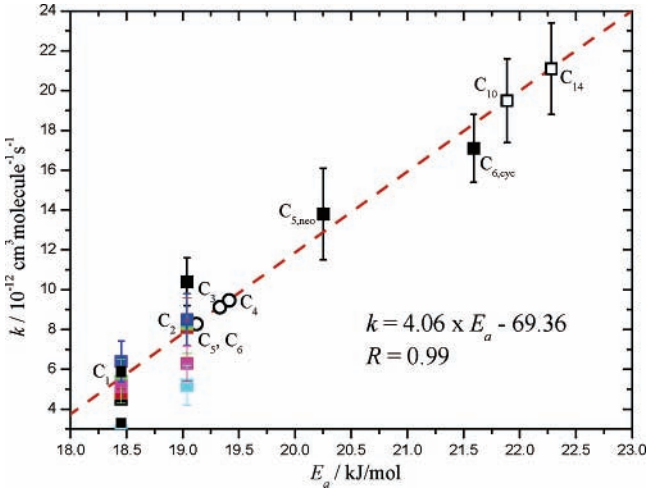

Figure 6. Least-squares linear correlation (the dashed line) of the room-temperature rate constants with the activation energies [E_a, calculated at the RCCSD(T)/cc-pVDZ//B3LYP6-311G(d,p) level of theory] for the reactions of HO_2 with $C_nH_mO_2$. The experimental data (refs 6−10, 26) denoted by the solid symbols were used in the fitting (weighted by the reported error bars). The hollow symbols denote the predicted data using the linear relationship.

IV. Concluding Remarks

The reaction mechanism of the $HO_2 + C_2H_5O_2$ reaction has been predicted using various ab initio levels of theory. The reaction takes place either on the triplet surface via a hydrogen abstraction route to form ethyl hydroperoxide (C_2H_5OOH) and oxygen molecules or on the singlet surface via an addition−elimination mechanism to form various radical products. Based on the ab initio computed energetic routes and the kinetic simulations, the triplet pathway plays a dominant role at low temperatures (e.g., below 300 K) and the addition−elimination mechanism on the singlet surface becomes important at higher temperatures.

Acknowledgment. This work was supported by A Foundation for the Author of National Excellent Doctoral Dissertation of PR China (FANEDD, 200224) and by the Scientific Research Foundation for the Returned Overseas Chinese Scholars, State Education Ministry.

Supporting Information Available: Figure S1 shows five high-barrier product channels for the $HO_2 + C_2H_5O_2$ reaction. Figure S2 shows the individual rate constants for the addition−elimination mechanism on the singlet surface. This material is available free of charge via the Internet at http://pubs.acs.org.

References and Notes

(1) Hou, H.; Wang, B. *J. Phys. Chem. A* **2005**, *109*, 451.
(2) Hou, H.; Deng, L.; Li, J.; Wang, B. *J. Phys. Chem. A* **2005**, *109*, 9299.
(3) Wallington, T. J.; Japar, S. M. *Chem. Phys. Lett.* **1990**, *166*, 495.
(4) Hasson, A. S.; Tyndall, G. S.; Orlando, J. J. *J. Phys. Chem. A* **2004**, *108*, 5979.
(5) Spittler, M.; Barnes, I.; Becker, K. H.; Wallington, T. J. *Chem. Phys. Lett.* **2000**, *321*, 57.
(6) Cattell, F. C.; Cavanagh, J.; Cox, R. A.; Jenkin, M. E. *J. Chem. Soc., Faraday Trans. 2* **1986**, *82*, 1999.
(7) Dagaut, P.; Wallington, T. J.; Kurylo, M. J. *J. Phys. Chem.* **1988**, *92*, 3836.
(8) Fenter, F. F.; Catoire, V.; Lesclaux, R.; Lightfoot, P. D. *J. Phys. Chem.* **1993**, *97*, 3530.
(9) Maricq, M. M.; Szente, J. J. *J. Phys. Chem.* **1994**, *98*, 2078.
(10) Boyd, A. A.; Flaud, P.-M.; Daugey, N.; Lesclaux, R. *J. Phys. Chem. A* **2003**, *107*, 818.
(11) (a) Becke, A. D. *J. Chem. Phys.* **1993**, *98*, 5648. (b) Lee, C.; Yang, W.; Parr, R. G. *Phys. Rev. B* **1988**, *37*, 785.
(12) Bartlett, R. J.; Purvis, G. D. *Int. J. Quantum Chem.* **1978**, *14*, 516.
(13) Woon, D. E.; Dunning, T. H., Jr. *J. Chem. Phys.* **1993**, *98*, 1358.
(14) Knowles, P. J.; Hampel, C.; Werner, H.-J. *J. Chem. Phys.* **1993**, *99*, 5219.
(15) Feller, D. *J. Chem. Phys.* **1992**, *96*, 6104.
(16) Helgaker, T.; Klopper, W.; Koch, H.; Noga, J. *J. Chem. Phys.* **1997**, *106*, 9639.
(17) Frisch, M. J.; et al. *Gaussian 03*, revision B.05; Gaussian Inc.: Pittburgh, PA, 2003.
(18) Werner, H.-J.; et al. MOLPRO, version 2002.6.
(19) Sander, S. P.; et al. *Chemical Kinetics and Photochemical Data for Use in Atmospheric Studies*; Evaluation Number 14, JPL Publication 02-25; Jet Propulsion Laboratory: Pasadena, CA, 2003.
(20) Moller, C.; Plesset, M. S. *Phys. Rev.* **1934**, *46*, 618.
(21) Gilbert, R. G.; Smith, S. C. *Theory of Unimolecular Reactions*; Blackwell Scientific: Carlton, Australia, 1990.
(22) (a) Klippenstein, S. J. *J. Phys. Chem.* **1994**, *98*, 11459. (b) Miller, W. H. *J. Am. Chem. Soc.* **1979**, *101*, 6810.
(23) Allen, M. P.; Tildesley, D. J. *Computer Simulation of Liquids*; Oxford Science Publications: Clarenden Press: Oxford, 1987; p 21, Table 1.1.
(24) Wardlaw, D. M.; Marcus, R. A. *Chem. Phys. Lett.* **1984**, *110*, 230.
(25) Klippenstein, S. J., et al. VARIFLEX: version 1.00, 1999.
(26) Kaiser, E. W. *Int. J. Chem. Kinet.* **1983**, *15*, 997; **1987**, *19*, 457.
(27) Kaiser, E. W. Private communications.
(28) Dagaut, P.; Wallington, T. J.; Kurylo, M. J. *J. Phys. Chem.* **1988**, *92*, 3833.
(29) Lightfoot, P. D.; Roussel, P.; Caralp, F.; Lesclaux, R. *J. Chem. Soc., Faraday Trans.* **1991**, *87*, 3213.
(30) Kurylo, M. J.; Dagaut, P.; Wallington, T. J.; Neuman, D. M. *Chem. Phys. Lett.* **1987**, *139*, 513.
(31) McAdam, K.; Veyret, B.; Lesclaux, R. *Chem. Phys. Lett.* **1987**, *133*, 39.
(32) Jenkin, M. E.; Cox, R. A.; Hayman, G. D.; Whyte, L. J. *J. Chem. Soc., Faraday Trans. 2* **1988**, *84*, 913.
(33) Moortgat, G. K.; Cox, R. A.; Schuster, G.; Burrows, J. P.; Tyndall, G. S. *J. Chem. Soc., Faraday Trans. 2* **1989**, *85*, 809.
(34) Lightfoot, P. D.; Veyret, B.; Lesclaux, R. *J. Phys. Chem.* **1990**, *94*, 708.
(35) Wallington, T. J. *J. Chem. Soc., Faraday Trans.* **1991**, *87*, 2379.
(36) Cox, R. A.; Tyndall, G. S. *J. Chem. Soc., Faraday Trans. 2* **1980**, *76*, 153.